THE STAR FORMATION RATE OF SUPERSONIC MAGNETOHYDRODYNAMIC TURBULENCE

Paolo Padoan[1] and Åke Nordlund[2]

[1] ICREA & Institut de Ciències del Cosmos (ICC), Universitat de Barcelona (IEEC-UB), Marti i Franquès 1, E08028 Barcelona, Spain; ppadoan@icc.ub.edu
[2] Niels Bohr Institute, University of Copenhagen, Juliane Maries Vej 30, DK-2100 Copenhagen, Denmark; aake@nbi.dk

ABSTRACT

This work presents a new physical model of the star formation rate (SFR), which is verified with an unprecedented set of large numerical simulations of driven, supersonic, self-gravitating, magneto-hydrodynamic (MHD) turbulence, where collapsing cores are captured with accreting sink particles. The model depends on the relative importance of gravitational, turbulent, magnetic, and thermal energies, expressed through the virial parameter, $\alpha_{\rm vir}$, the rms sonic Mach number, $\mathcal{M}_{\rm S,0}$, and the ratio of mean gas pressure to mean magnetic pressure, β_0. The SFR is predicted to decrease with increasing $\alpha_{\rm vir}$ (stronger turbulence relative to gravity), to increase with increasing $\mathcal{M}_{\rm S,0}$ (for constant values of $\alpha_{\rm vir}$), and to depend weakly on β_0 for values typical of star forming regions ($\mathcal{M}_{\rm S,0} \approx 4$–20 and $\beta_0 \approx 1$–20). In the unrealistic limit of $\beta_0 \to \infty$, that is, in the complete absence of a magnetic field, the SFR increases approximately by a factor of three, which shows the importance of magnetic fields in the star formation process, even when they are relatively weak (super-Alfvénic turbulence). The star-formation simulations used to test the model result in an approximately constant SFR, after an initial transient phase. The dependence of the SFR on the virial parameter is shown to agree very well with the theoretical predictions.

Key words: ISM: kinematics and dynamics – magnetohydrodynamics (MHD) – stars: formation – turbulence

Online-only material: color figures

1. INTRODUCTION

A physical theory of the star formation rate (SFR) should explain why the star formation process is slow, meaning that it converts only a small fraction of the gas mass into stars in a free-fall time, $\tau_{\rm ff}$, both on Galactic scale (Zuckerman & Palmer 1974; Williams & McKee 1997) and on the scale of individual clouds (Krumholz & Tan 2007; Evans et al. 2009). Several authors have proposed that the observed supersonic turbulence may be responsible for keeping the SFR low by providing turbulent pressure support against the gravitational collapse. For example, Bonazzola et al. (1987, 1992) presented a gravitational instability analysis that includes the effect of local turbulent pressure support; Krumholz & McKee (2005) defined the critical density for star formation based on the local turbulent pressure support of a Bonnor–Ebert sphere; and Hennebelle & Chabrier (2008) proposed that the Salpeter stellar initial mass function (IMF) is the result of the local turbulent pressure support. In all these works, the turbulent pressure is assumed to scale according to the observed Larson velocity–size relation (Larson 1981; Heyer & Brunt 2004) or by numerical simulations.

The concept of turbulent pressure support was introduced in the context of subsonic, small-scale turbulence by Chandrasekhar (1951). It applies when the two following conditions are satisfied, $L \ll L_{\rm J}$ and $\sigma_{\rm v} \ll c_{\rm S}$, where L is the length scale, $L_{\rm J}$ is the Jeans length, $\sigma_{\rm v}$ is the velocity dispersion, and $c_{\rm S}$ is the sound speed. In the supersonic turbulence of star-forming regions, both conditions are violated. As a result, the turbulence can actually trigger gravitational collapse, causing a large-scale compression rather than preventing it. The turbulence is responsible for much of the complex and filamentary density structure observed in molecular clouds, and prestellar cores are likely assembled as the densest regions in this turbulent fragmentation process (Padoan et al. 2001). However, even though supersonic turbulence is able to intermittently create dense regions that are gravitationally unstable, it does so only inefficiently, and its net effect on the large scale is that of suppressing star formation when the total turbulent kinetic energy exceeds the total gravitational energy.

Focusing on the competition between supersonic turbulence and self-gravity, the star formation process can be shown to depend primarily on the ratio of the turbulent kinetic energy, $E_{\rm K}$, and the gravitational energy, $E_{\rm G}$, of a star-forming region. This ratio may be measured by the virial parameter introduced by Bertoldi & McKee (1992)

$$\alpha_{\rm vir} \sim \frac{2E_{\rm K}}{E_{\rm G}} = \frac{5\sigma_{\rm v,1D}^2 R}{GM}, \qquad (1)$$

where $\sigma_{\rm v,1D}$ is the one-dimensional rms velocity, R and M are the cloud radius and mass, respectively, and G is the gravitational constant, and it has been assumed that the cloud is a sphere with uniform density. If the dynamical time is defined as the ratio of the cloud radius and the three-dimensional rms velocity, $\tau_{\rm dyn} = R/\sigma_{\rm v,3D}$, and using the standard definition of the free-fall time, $\tau_{\rm ff,0} = (3\pi/(32G\rho_0))^{1/2}$, the virial parameter can also be expressed as

$$\alpha_{\rm vir} = 0.7(\tau_{\rm ff,0}/\tau_{\rm dyn})^2. \qquad (2)$$

Krumholz & McKee (2005) derived a theoretical model where the SFR is primarily controlled by the virial parameter. In this model, it is assumed that the gas mass above some critical density, $\rho_{\rm cr}$, is gravitationally unstable, and the fraction of this unstable mass is computed assuming the gas density obeys a lognormal pdf (Nordlund & Padoan 1999). Following Padoan (1995), the critical density is defined through the comparison of the Jeans' length and the sonic scale, $\lambda_{\rm s}$, which is the scale where the turbulent velocity differences are of the order of the speed of sound. The critical density is equivalent to that of the critical Bonnor–Ebert mass of size $\lambda_{\rm s}$. The idea of relying on the density pdf was also exploited in Padoan & Nordlund (2002, 2004) to explain the stellar IMF and the origin of brown dwarfs, and by Padoan (1995) to model the SFR.

The model of Krumholz & McKee (2005) was calibrated and tested using low-resolution SPH simulations by Vázquez-Semadeni et al. (2003). Because of the important role of turbulent energy in this model, low-resolution simulations are inadequate. They do not develop an inertial range of turbulence and are expected to produce a too large SFR—which they do, as recognized in a later paper, based on higher-resolution grid simulations, by some of the same authors (Vázquez-Semadeni et al. 2005). However, Krumholz & McKee (2005) estimated a rather low SFR from the simulations of Vázquez-Semadeni et al. (2003) by fitting only their early evolution. We argue that this is a transient phase of accelerated SFR and should not be used to test the model (although it cannot be excluded that real molecular clouds experience such a phase of accelerated star formation, the initial transient phase in the simulations is of numerical origin, due to the sudden inclusion of self-gravity in our case, or to the memory of artificial initial conditions in Vázquez-Semadeni et al. 2003, where gravity is included from the beginning). A new set of larger simulations is needed to properly test the theoretical model. Because the model by Krumholz & McKee (2005) does not include the effect of magnetic fields, a new model based on MHD turbulence should be derived, and this new MHD model should be tested with large numerical simulations as well.

In this work, we propose such a new MHD model of the SFR, and we test it with an unprecedented set of large numerical simulations of driven, supersonic, self-gravitating, MHD turbulence, where collapsing cores are represented by accreting sink particles. Both the model and the simulations are limited to the case of an isothermal gas, and the effect of deviations from the isothermal behavior is not addressed. To model the process of star formation, we must include gravitational, turbulent, magnetic, and thermal energies. Here, we express their relative importance through the virial parameter, α_{vir}, the rms sonic Mach number, $\mathcal{M}_{S,0}$, and the mean gas pressure to mean magnetic pressure, β_0, and we derive a model that depends explicitly on all three non-dimensional parameters. In the non-magnetized limit of $\beta_0 \to \infty$, our definition of the critical density for star formation has the same dependence on α_{vir} and $\mathcal{M}_{S,0}$ as in the model of Krumholz & McKee (2005), but our derivation does not rely on the concepts of local turbulent pressure support and sonic scale as in that work. However, even in this non-magnetized case, our model predicts a different dependence of the SFR on α_{vir} and $\mathcal{M}_{S,0}$ from the model of Krumholz & McKee (2005), because we assume that regions exceeding the critical density turn into stars on a timescale given by their local free-fall time, rather than the free-fall time of the mean density.

Although the non-magnetized case can be derived from our MHD model in the limit of $\beta_0 \to \infty$, we structure the paper by first deriving the critical density in the purely hydrodynamic (HD) case (Section 2), and then in the general MHD case (Section 3). Likewise, in Section 4, we first present a simple model for the density pdf in the HD case, and then generalize the approach to MHD turbulence. In Section 5, we derive the model predictions for the SFR and in Section 6, we present our numerical simulations of HD and MHD self-gravitating turbulence. The comparison between the model and the simulations is presented in Section 7, results are discussed in Section 8, and conclusions are summarized in Section 9.

2. CRITICAL DENSITY IN HYDRODYNAMIC TURBULENCE

In the HD case, the main source of pressure in the postshock gas is the thermal pressure, so the shock jump conditions are given by the balance of thermal pressure and ram pressure:

$$\rho_{HD}\, c_S^2 = \rho_0 (v_0/2)^2, \tag{3}$$

where c_S is the sound speed, ρ_0 and ρ_{HD} are the preshock and postshock gas densities, and $v_0/2$ is the shock velocity. Because we use this equation to estimate a characteristic postshock density in the HD case, ρ_{HD}, we choose the mean gas density, ρ_0, as the preshock density, and half the rms velocity, v_0, as the shock velocity. Assuming an ensemble of eddies with a randomly oriented velocity of mean magnitude v_0, the average collision velocity is also v_0. However, the shock velocity is half of that average collision velocity because the postshock layer is confined by two shocks, each with velocity $v_0/2$. The characteristic density is then given by

$$\rho_{HD} = \rho_0 \mathcal{M}_{S,0}^2 / 4, \tag{4}$$

where $\mathcal{M}_{S,0}$ is the rms sonic Mach number, and the characteristic thickness, λ_{HD}, of the postshock layers is

$$\lambda_{HD} = (\theta\, L_0)\, 4 / \mathcal{M}_{S,0}^2, \tag{5}$$

where L_0 is the size (e.g., the diameter for a sphere) of the system and $\theta\, L_0$, with $\theta \leqslant 1$, is the turbulence integral scale. Because the turbulence velocity scaling is approximately $v \propto \ell^{1/2}$, this characteristic thickness is practically scale independent (it would have been the same if derived at any other scale, not only at the integral scale). The local condition for collapse is that $M_{HD}(\rho) \geqslant M_{BE}(\rho)$, where M_{BE} is the Bonnor–Ebert mass (Bonnor 1956; Ebert 1957) with external density equal to the postshock density ρ,

$$M_{BE} = 1.182\, c_S^3 / (G^{3/2} \rho^{1/2}) \tag{6}$$

and M_{HD} is the mass of a uniform sphere of radius $\lambda_{HD}/2$, $M_{HD}(\rho) = (4/3)\pi (\lambda_{HD}/2)^3\, \rho$.

Because the thickness, λ_{HD}, is scale independent, the condition for collapse can be used to define a scale-independent critical density for collapse. The local density depends on the distribution of local shock velocity and preshock density and is known to follow a lognormal pdf (Vazquez-Semadeni 1994; Padoan et al. 1997; Nordlund & Padoan 1999; Ostriker et al. 2001; Li et al. 2004; Kritsuk et al. 2007; Beetz et al. 2008; Lemaster & Stone 2008; Federrath et al. 2008), so there is a finite probability that a region exceeds the critical density and undergoes collapse. We therefore define the critical density for star formation, $\rho_{cr,HD}$, as the minimum density that satisfies the local condition for collapse:

$$M_{HD}(\rho_{cr,HD}) = M_{BE}(\rho_{cr,HD}) \tag{7}$$

which yields

$$\rho_{cr,HD}/\rho_0 = 0.067\, \theta^{-2} \alpha_{vir}\, \mathcal{M}_{S,0}^2, \tag{8}$$

where α_{vir} is the virial parameter defined above in Equation (1) and can be re-written as

$$\alpha_{vir} = 5 v_0^2 / (\pi\, G \rho_0 L_0^2), \tag{9}$$

assuming the system is a uniform sphere of radius $L_0/2$, mean gas density ρ_0, and three-dimensional rms turbulent velocity v_0.

The critical density defined by Equation (8) has the same dependence on α_{vir} and almost the same dependence on $\mathcal{M}_{S,0}$

as the critical density derived by Krumholz & McKee (2005). However, the critical density has been derived here without any reference to the concepts of turbulent pressure support and sonic scale. On the contrary, our derivation is based on the idea that the turbulence is a trigger of local gravitational instabilities through its dynamical pressure. This physical difference between the two derivations is reflected by the Mach number dependence. In Krumholz & McKee (2005), $\rho_{\rm cr,HD} \sim \mathcal{M}_{\rm S,0}^{2/p-2}$, where p is the exponent of the velocity–size relation, $v \propto \ell^p$, which gives the same dependence on Mach number as in our model, $\rho_{\rm cr,HD} \sim \mathcal{M}_{\rm S,0}^2$, only for the specific value of $p = 1/2$. In supersonic turbulence, however, the scaling exponent is not necessarily identical to the Burgers value of $p = 1/2$. Numerical simulations yield somewhat smaller values based on the second-order velocity structure functions, or somewhat larger ones based on the first order (Kritsuk et al. 2007).

The ratio between the characteristic density, $\rho_{\rm HD}$, and the critical density, $\rho_{\rm cr,HD}$, is independent of $\mathcal{M}_{\rm S,0}$,

$$\rho_{\rm HD}/\rho_{\rm cr,HD} = 3.521\,\theta^2 \alpha_{\rm vir}^{-1}, \qquad (10)$$

which anticipates the result that the mass fraction with density above $\rho_{\rm cr,HD}$ (and hence the SFR) must have a rather weak Mach number dependence (despite the strong dependence of $\rho_{\rm cr,HD}$ on $\mathcal{M}_{\rm S,0}$) and must increase with decreasing $\alpha_{\rm vir}$ (weaker turbulence relative to gravity).

In numerical simulations, the integral scale of the turbulence is somewhat smaller than the system size ($\theta < 1$). For example, in our simulations of supersonic turbulence driven in the range of wavenumbers $1 \leqslant k \leqslant 2$ ($k = 1$ corresponds to the box size), $\theta \approx 0.35$ (including a correction factor discussed in Wang & George 2002). We adopt this value of θ when we compare the models with the simulations in Section 7. If star-forming regions are driven on very large scales, for example by the expansion of supernova remnants (Korpi et al. 1999; Kim et al. 2001; de Avillez & Breitschwerdt 2005; Joung & Mac Low 2006; Tamburro et al. 2009), the turbulence integral scale could be much larger than the size of individual star-forming regions. However, in our model θL_0 is the characteristic scale of regions of compression with velocity of order the flow rms velocity, v_0, with v_0 being measured within the region of size L_0. We therefore adopt the same value of $\theta = 0.35$ as estimated in the simulations. With $\theta = 0.35$, the critical number density is

$$n_{\rm cr,HD}/n_0 = 0.547\,\alpha_{\rm vir} \mathcal{M}_{\rm S,0}^2. \qquad (11)$$

Adopting characteristic parameters of molecular clouds on a scale of 10 pc, $\alpha_{\rm vir} \approx 1.6$, $n_0 \approx 200$ cm^{-3}, and $\mathcal{M}_{\rm S,0} \approx 20$, we get a characteristic number density of $n_{\rm HD} \approx 2.0 \times 10^4$ cm^{-3} from Equation (4), reasonable for prestellar cores, and a factor of 3.5 below the critical number density, $n_{\rm cr,HD} \approx 350.1\,n_0 \approx 7.0 \times 10^4$ cm^{-3}. The critical overdensity factor of 350.1 is somewhat larger than the value of 275 derived from Equation (27) of Krumholz & McKee (2005), using the same values of $\alpha_{\rm vir}$ and $\mathcal{M}_{\rm S,0}$ (note that their Mach number is one dimensional, so a factor of $3^{1/2}$ smaller than ours) and assuming $\phi_x = 1.12$ for their numerical coefficient (their best fit to numerical simulations).

3. CRITICAL DENSITY IN MHD TURBULENCE

We now consider the MHD case. Including both thermal and magnetic pressures, and using $v_0/2$ for the shock velocity, as in

Equation (3), the pressure balance condition for MHD shocks is

$$\rho_{\rm MHD}\left(c_{\rm S}^2 + v_{\rm A}^2/2\right) = \rho_0(v_0/2)^2, \qquad (12)$$

where $v_{\rm A}$ is the Alfvén velocity in the postshock gas defined by the postshock magnetic field perpendicular to the direction of compression. Because the field is amplified only in the direction perpendicular to the compression, the postshock perpendicular field is comparable to the total postshock field,[3] and we can write, $v_{\rm A} \approx B/(4\pi\rho)^{1/2}$, where B is the postshock magnetic field and ρ is the postshock gas density. The characteristic gas density and thickness of postshock layers are thus given by

$$\rho_{\rm MHD} = \rho_0\left(\mathcal{M}_{\rm S,0}^2/4\right)(1 + \beta^{-1})^{-1}, \qquad (13)$$

$$\lambda_{\rm MHD} = (\theta\,L_0)\left(\mathcal{M}_{\rm S,0}^2/4\right)^{-1}(1 + \beta^{-1}), \qquad (14)$$

where we have introduced the ratio of gas to magnetic pressure in the postshock gas, $\beta = 2\,c_{\rm S}^2/v_{\rm A}^2$. In the limit of $\beta \to \infty$, these expressions reduce to the corresponding HD ones, given by Equations (4) and (5). The value of $\lambda_{\rm MHD}$ is not scale independent. Its scale dependence is at the heart of the relation between the exponent of the Salpeter stellar IMF and the turbulent velocity power spectrum, in the IMF model of Padoan & Nordlund (2002). However, we can still define a characteristic thickness, and hence a characteristic critical density, as in the HD case, because the average postshock Alfvén velocity, $v_{\rm A}$ (and the corresponding postshock β), is only very weakly dependent on density. In numerical simulations of supersonic and super-Alfvénic turbulence, it is found that, although $v_{\rm A}$ has a very large scatter for any given density, its mean value is nearly density independent, corresponding to a mean relation approaching $B \propto \rho^{1/2}$ for a very weak mean magnetic field (Padoan & Nordlund 1999). In the specific MHD simulation used in this work, the mean value of $v_{\rm A}$ is almost exactly constant for any density $\rho \gtrsim 2\rho_0$ (see Figure 1). Zeeman splitting measurements of the magnetic field strength in molecular cloud cores are also consistent with an average value of $v_{\rm A}$ nearly independent of density (Crutcher 1999).

As in the HD case, we define the critical density as the density above which a uniform sphere of radius $\lambda_{\rm MHD}/2$ is gravitationally unstable, assuming that variations in the thickness around $\lambda_{\rm MHD}$ are not strongly correlated with the density variations. To account for both thermal and magnetic support, we adopt the approximation of the critical mass for collapse, $M_{\rm cr}$, introduced by McKee (1989),

$$M_{\rm cr} \approx M_{\rm BE} + M_\phi, \qquad (15)$$

where M_ϕ is the magnetic critical mass for a sphere of radius R, mean density equal to the postshock density ρ, and constant mass-to-flux ratio

$$M_\phi = 0.17\pi R^2 B/G^{1/2} = 0.387 v_{\rm A}^3/(G^{3/2}\rho^{1/2}), \qquad (16)$$

where the numerical coefficient 0.17 is from Tomisaka et al. (1988; see also Nakano & Nakamura 1978 for the case of an

---

[3] For the magnetic field strength in the postshock gas, we can write $B_\perp^2 = B^2 - B_\parallel^2 = B^2 - B_{0,\parallel}^2$, where the second equality is from the fact that the component parallel to the direction of the compression is not amplified. If we take an average, assuming a random orientation of the magnetic field relative to the direction of compression, we get $\langle B_\perp^2 \rangle = \langle B^2 \rangle - B_0^3/3$, and hence $\langle B_\perp^2 \rangle/\langle B^2 \rangle = 1 - (B_0^2/\langle B^2 \rangle)/3$. Thus, on average, the relative error in β as a result of assuming $B = B_\perp$ is $(B_0^2/\langle B^2 \rangle)/3$, which is typically of order 1% or less.
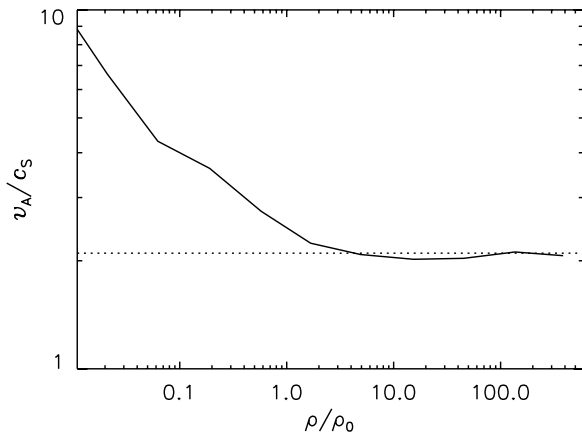
Figure 1. Mean Alfvén velocity, in units of the sound speed, vs. gas density, in units of the mean density, for a snapshot of the 1000^3 MHD turbulence simulation prior to the inclusion of self-gravity. The Alfvén velocity is essentially independent of density for densities above the mean. The dotted line shows the mean value of 0.21, computed for densities larger than twice the mean.

infinite sheet, and McKee & Ostriker 2007 for a discussion of ellipsoidal clouds and other geometries). The critical density is defined by the condition

$$M_{\mathrm{MHD}}(\rho_{\mathrm{cr,MHD}}) = M_{\mathrm{BE}}(\rho_{\mathrm{cr,MHD}}) + M_\phi(\rho_{\mathrm{cr,MHD}}), \qquad (17)$$

where $M_{\mathrm{MHD}}(\rho) = (4/3)\pi(\lambda_{\mathrm{MHD}}/2)^3\rho$. Equation (17) results in the following expression for the critical density as a function of the three non-dimensional parameters, α_{vir}, $\mathcal{M}_{\mathrm{S,0}}$, and β:

$$\frac{\rho_{\mathrm{cr,MHD}}}{\rho_0} = 0.067\,\theta^{-2}\alpha_{\mathrm{vir}}\,\mathcal{M}_{\mathrm{S,0}}^2\,\frac{\left(1 + 0.925\beta^{-\frac{3}{2}}\right)^{\frac{2}{3}}}{(1 + \beta^{-1})^2}, \qquad (18)$$

which is smaller than $\rho_{\mathrm{cr,HD}}$ for any value of β, and reduces to the expression for $\rho_{\mathrm{cr,HD}}$ given by Equation (8), in the limit of $\beta \to \infty$. The relative ratio of characteristic to critical density in MHD and HD is given by the following function of β:

$$\frac{\rho_{\mathrm{MHD}}/\rho_{\mathrm{cr,MHD}}}{\rho_{\mathrm{HD}}/\rho_{\mathrm{cr,HD}}} = \frac{(1 + \beta^{-1})}{\left(1 + 0.925\beta^{-\frac{3}{2}}\right)^{\frac{2}{3}}}. \qquad (19)$$

This ratio is slightly larger than unity for any value of β (with a maximum of ≈ 1.3 at $\beta \approx 0.86$), suggesting that star formation should be slightly more likely in MHD turbulence than in the HD case. However, due to the less broad gas density pdf in the MHD case (see the next section), the net result is instead a lower SFR in MHD than in HD.

We have verified that the average value of β is nearly independent of density in the MHD simulation used to generate the initial condition for the MHD star formation simulations described in Section 6. In that simulation, the rms sonic Mach number is $\mathcal{M}_{\mathrm{S,0}} \approx 9$ and the mean Alfvén velocity is $v_{\mathrm{A,0}} = 0.3\,c_{\mathrm{S}}$, computed with the mean density and mean magnetic field. However, the rms magnetic field is amplified by the turbulence, so the actual Alfvén velocity should be computed as the local absolute value of B divided by the local value of the density, which gives $v_{\mathrm{A}} = \langle|B|/(4\pi\rho)^{1/2}\rangle = 2.1\,c_{\mathrm{S}}$, if averaged over all regions with density larger than twice the mean (the Alfvén velocity introduced in Equation (12) is measured in the postshock gas, so it should be estimated as an average in overdense regions). Figure 1 shows the mean Alfvén velocity

as a function of the gas density in the snapshot used as the initial condition for the MHD star formation simulations (see Section 6). The Alfvén velocity is almost exactly constant at densities above the mean.

In numerical simulations of super-Alfvénic turbulence, the rms magnetic field is the result of the amplification of some weak initial field by compressions and, possibly, by a turbulent dynamo. These simulations typically start from an initially uniform field, B_0, which is also the conserved mean magnetic field. It would be useful to relate our postshock β to the ratio of gas to magnetic pressure computed with the mean magnetic field, B_0, and the mean gas density, ρ_0, $\beta_0 = 2\,c_{\mathrm{S}}^2/v_{\mathrm{A,0}}^2$, where $v_{\mathrm{A,0}}^2 = B_0^2/(4\pi\rho_0)$. An approximate relation for the dependence of β on β_0 and $\mathcal{M}_{\mathrm{S,0}}$ can be derived based on flux freezing, on the simplified MHD shock jump conditions without thermal pressure (where we assume that the characteristic shock velocity is $v_0/2$, as in Equations (3) and (12)), and neglecting dynamical alignment of flow velocity and magnetic field:

$$\beta \approx b\,\beta_0^{1/2}\mathcal{M}_{\mathrm{S,0}}^{-1}. \qquad (20)$$

With the MHD simulation of this work, we derive $b = 0.22$ when β is computed from the mean-squared value of v_{A} averaged over the whole computational box (not limited to overdense regions). We find that Equation (20) is a very good approximation also for the three 1024^3 simulations of Kritsuk et al. (2009a), where $\mathcal{M}_{\mathrm{S,0}} \approx 10$ and $\beta_0 = 0.2$, 2, and 20 (it overestimates β by approximately 20% for $\beta_0 = 0.2$ and 2.0, and underestimates it by approximately 2% for $\beta_0 = 20$). However, if β is computed from the mean-squared v_{A} averaged above a certain density, we find that, as we increase the value of that density threshold, the value of β becomes gradually independent of β_0. For densities larger than 50 times the mean, for example, all three simulations yield $\beta \approx 1$. This can be understood as due to the tendency of the strongest density enhancements to originate from compressions along the magnetic field direction. This tendency becomes stronger for decreasing values of $\mathcal{M}_{\mathrm{A,0}}$, or, at constant $\mathcal{M}_{\mathrm{S,0}}$, for decreasing values of β_0, as documented by the increased alignment of flow velocity and magnetic field (Kritsuk et al. 2009b).

Given the difficulty of deriving a robust value of the effective postshock β to be used in the model for the critical density, we estimate β based on the density pdf, as explained in the next section. We will derive a value of $\beta = 0.39$. The compilations of OH and CN Zeeman measurements by Troland & Crutcher (2008) and Falgarone et al. (2008) give an average value of $\beta = 0.34$ and 0.28, respectively, using the line-of-sight magnetic field strength of their 3σ detections, assuming a temperature $T = 10$ and 50 K, respectively, and averaging the values of β of the individual cores. These estimated values of β are very close to that derived in the next section based on the density pdf.

4. GAS DENSITY PDF

We can estimate the gas mass fraction that is turned into stars by computing the mass fraction above the critical density, as in Krumholz & McKee (2005). For given values of α_{vir}, $\mathcal{M}_{\mathrm{S,0}}$, and β (or β_0), the critical density is fixed, and the mass fraction above the critical density is determined by the density pdf. In the HD case, the density pdf is known to be lognormal, with a standard deviation depending on the rms Mach number. Following the numerical results of Padoan et al. (1997) for the Mach number

dependence, the pdf is given by

$$p_{HD}(x)dx = \frac{x^{-1}}{\left(2\pi\sigma_{HD}^2\right)^{1/2}} \exp\left[-\frac{\left(\ln x + \sigma_{HD}^2/2\right)^2}{2\,\sigma_{HD}^2}\right]dx \quad (21)$$

and the standard deviation, σ, is given by

$$\sigma_{HD}^2 \approx \ln\left[1 + \left(\frac{\mathcal{M}_{S,0}}{2}\right)^2\right]. \quad (22)$$

Equation (22) for the standard deviation of the logarithm of the overdensity, $\ln x$, implies a simple expression for the standard deviation, $\sigma_{x,HD}$, of the overdensity, x,

$$\sigma_{x,HD} \approx \mathcal{M}_{S,0}/2. \quad (23)$$

In the MHD case, the density pdf may deviate from the lognormal and it may depend on both the sonic and the Alfvénic Mach numbers. Lemaster & Stone (2008) have shown that the density pdf in supersonic MHD simulations with a strong field, corresponding to a mean value of $\beta_0 = 0.02$, is very similar to the density pdf in the HD case. Assuming a lognormal pdf, the averaged results given in their Table 1 correspond to the relation $\sigma_{x,MHD} \approx C\,\mathcal{M}_{S,0}/2$, with $C \approx 0.8$ at $\mathcal{M}_{S,0} < 4$, and C decreasing with increasing Mach number for $\mathcal{M}_{S,0} > 4$. In their largest Mach number run, they find $C \approx 0.66$ with $\mathcal{M}_{S,0} \approx 6.7$, not far from the value of $C \approx 0.53$ derived below (see Equation (29)) from our MHD run with an even larger Mach number, $\mathcal{M}_{S,0} \approx 9$. In the absence of a detailed numerical study, including different values of β_0 and large values of $\mathcal{M}_{S,0}$, here we derive a simple model for the density pdf in the MHD case, based on arguments inspired by the HD case. We assume that the pdf can be approximated by a lognormal also in the MHD case,

$$p_{MHD}(x)dx = \frac{x^{-1}}{\left(2\pi\sigma_{MHD}^2\right)^{1/2}} \exp\left[-\frac{\left(\ln x + \sigma_{MHD}^2/2\right)^2}{2\,\sigma_{MHD}^2}\right]dx$$
$$(24)$$

at least in the super-Alfvénic regime that we think is relevant for molecular clouds (Padoan & Nordlund 1999; Lunttila et al. 2008, 2009). This may not be a good approximation for the low-density tail of the pdf, but for the present purpose we are primarily interested in the high-density tail. To derive an expression for σ_{MHD}, we first show that the dependence of σ_{HD} on $\mathcal{M}_{S,0}$ can be obtained with a simple derivation, and we then apply the same derivation to the MHD case.

Let us consider a cubic box of size L_0 swept by a single compression of sonic Mach number $\mathcal{M}_{S,0}$ in one direction and therefore accumulating all the mass in a postshock layer of size L_0 and density and thickness given by Equations (4) and (5), respectively, with $\theta = 1$. The standard deviation of the density, σ_ρ, is given by

$$\sigma_\rho^2 = \frac{1}{V}\int_V (\rho - \rho_0)^2 dV, \quad (25)$$

where V is the volume, and the integral is over the whole volume. In our simple model, the density is either zero outside of the layer, or $\rho = \rho_{HD} \gg \rho_0$ inside the layer. The integral is therefore approximately equal to ρ_{HD}^2 times the volume of the layer, V_{layer},

$$\sigma_\rho^2 \approx \frac{1}{V}\left(\rho_{HD}^2 V_{layer}\right) = \frac{\lambda_{HD}L_0^2}{L_0^3}\rho_{HD}^2 = \rho_0^2\mathcal{M}_{S,0}^2/4, \quad (26)$$

where we have used Equations (4) and (5) in the last equality. This result is equivalent to Equation (23) which was derived from numerical simulations of supersonic turbulence (Padoan et al. 1997; Nordlund & Padoan 1999), and was recently confirmed by Brunt et al. (2010), based on extinction maps of the Taurus molecular cloud. Following the same derivation in the MHD case, we obtain

$$\sigma_{x,MHD} \approx (1 + \beta^{-1})^{-1/2}\mathcal{M}_{S,0}/2 \quad (27)$$

corresponding to

$$\sigma_{MHD}^2 \approx \ln\left[1 + \left(\frac{\mathcal{M}_{S,0}}{2}\right)^2(1 + \beta^{-1})^{-1}\right]. \quad (28)$$

As explained at the end of the previous section, we cannot rely on Equation (20) to derive the effective postshock β from the values of β_0 and $\mathcal{M}_{S,0}$. This is further illustrated by the fact that the density pdfs in the three 1024^3 simulations of Kritsuk et al. (2009a; where $\mathcal{M}_{S,0} \approx 10$ and $\beta_0 = 0.2$, 2, and 20) are almost indistinguishable from each other, for densities above the peak of the pdfs. This is again interpreted as due to the growing tendency of large density enhancements to result from compressions parallel to the magnetic field, as the mean magnetic field strength increases, or the value of β_0 decreases. Based on our model for the standard deviation of the pdf, Equation (27), the fact that the pdf does not change with β_0 implies that β is independent of β_0. We fit this simple pdf model to the actual density pdf of our MHD run to derive the corresponding β. The functional form of Equation (28) should be confirmed by numerical simulations. However, this equation has been derived under the same assumptions, and using the same meaning of the postshock β, as in the derivation of the critical density. This justifies our approach of deriving β by fitting the density pdf.

Figure 2 compares the HD and MHD model pdfs to the actual pdfs of the snapshots used as initial conditions for the star formation simulations. The MHD model provides an excellent fit to the high-density tail of the pdf, for over five orders of magnitude in probability. At the highest densities, the HD model predicts a slightly larger probability than in the HD simulation, a discrepancy that may be attributed to the limited numerical resolution, and would likely be reduced if the numerical pdf were the result of a time average of many snapshots (which would also improve the fit of the low-density tail of the pdf). The best fit to the MHD pdf is obtained with $\beta = 0.39$. We therefore adopt this value as the postshock β of our model for $\mathcal{M}_{S,0} \approx 10$ and $0.2 \lesssim \beta_0 \lesssim 20$.

Based on Equation (27), this value of β gives

$$\sigma_{x,MHD} \approx 0.53\,\mathcal{M}_{S,0}/2 \approx 0.53\,\sigma_{x,HD.} \quad (29)$$

We then speculate that β becomes independent of β_0, as β_0 is increased, as soon as the postshock magnetic pressure becomes important, because if it were not important, there would not be a significant alignment of flow velocity and magnetic field in regions of compression. Based on the simple approximations leading to Equation (20), the postshock magnetic pressure is of the order of the postshock thermal pressure, or larger, if $\mathcal{M}_{A,0} \gtrsim \sqrt{2}\beta_0$. This condition is satisfied by the three simulations of Kritsuk et al. (2009a).

In summary, we make the ansatz that the critical density and the standard deviation of the density pdf are given by
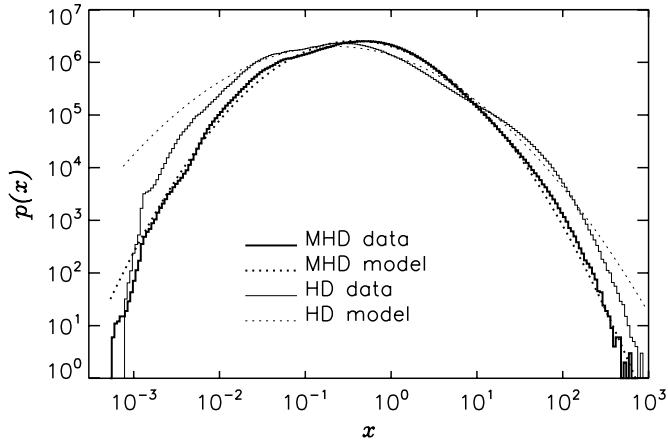
Figure 2. Pdf of gas density for the MHD and HD snapshots used as initial conditions for the star formation simulations (solid lines). The lognormal models used in this work are also shown (dotted lines).

Equations (18) and (27), respectively, where $\beta \approx 0.39$ if $\mathcal{M}_{A,0} \gtrsim \sqrt{2}\,\beta_0$, which covers all reasonable values of magnetic field strengths and Mach numbers in molecular clouds. If $\mathcal{M}_{A,0} < \sqrt{2}\,\beta_0$, then $\beta \to \infty$ as $\beta_0 \to \infty$, and both equations reduce to their corresponding non-magnetized forms, given by Equations (8) and (23), respectively.

5. STAR FORMATION RATE

In Padoan & Nordlund (2004), we computed the mass fraction available to form brown dwarfs as the integral of the pdf of gas density from a critical density to infinity. In that case, the critical density was defined as the density of a critical Bonnor–Ebert sphere with a mass of 0.075 $M_\odot$. Krumholz & McKee (2005) used the same integral to compute the total mass available for star formation and defined the critical density based on the condition of turbulent support of a Bonnor–Ebert sphere. Here we follow the same procedure, with the critical density defined by the condition for magnetic and thermal support expressed by Equation (17).

Assuming that a fraction ϵ of the mass fraction above the critical density is turned into stars in a free-fall time of the critical density, $\tau_{\mathrm{ff,cr}} = (3\pi/(32 G \rho_{\mathrm{cr,MHD}}))^{1/2}$, the SFR per free-fall time (the mass fraction turned into stars in a free-fall time) is given by[4]

$$
\begin{aligned}
\mathrm{SFR}_{\mathrm{ff}} &= \epsilon\, \frac{\tau_{\mathrm{ff,0}}}{\tau_{\mathrm{ff,cr}}} \int_{x_{\mathrm{cr}}}^{\infty} x\, p_{\mathrm{MHD}}(x)\, dx \\
&= \epsilon\, \frac{x_{\mathrm{cr}}^{1/2}}{2} \left(1 + \mathrm{erf}\left[\frac{\sigma^2 - 2\ln(x_{\mathrm{cr}})}{2^{3/2}\,\sigma} \right] \right)
\end{aligned}
\tag{30}
$$

where $\tau_{\mathrm{ff,0}} = (3\pi/(32 G \rho_0))^{1/2}$ is the free-fall time of the mean density, $x_{\mathrm{cr}} = \rho_{\mathrm{cr,MHD}}/\rho_0$ given by Equation (18), $\sigma = \sigma_{\mathrm{MHD}}$ given by Equation (28), and the expression is valid also in the limit of $\beta \to \infty$.

Krumholz & Tan (2007) have argued that the value of $\mathrm{SFR}_{\mathrm{ff}}$ is approximately the same in very different star-forming environ-

ments. If so, the choice of expressing the SFR with a time unit equal to the free-fall time, introduced in Krumholz & McKee (2005), is useful when comparing with observational estimates of the SFR. However, if star-forming clouds on all scales were mostly transient structures, surviving only a few local dynamical times in the turbulent flow that formed them, observational estimates of the star formation efficiency (SFE; rather than the SFR) could be compared directly with the predicted SFR per dynamical time, $\mathrm{SFR}_{\mathrm{dyn}} = \mathrm{SFR}_{\mathrm{ff}}\,\tau_{\mathrm{dyn}}/\tau_{\mathrm{ff,0}}$, where $\tau_{\mathrm{dyn}} = R/\sigma_{v,\mathrm{3D}}$, and R is the cloud radius. With this definition of the dynamical time as a crossing time, $\mathrm{SFR}_{\mathrm{dyn}}$ decreases with increasing α_{vir} faster than $\mathrm{SFR}_{\mathrm{ff}}$, $\mathrm{SFR}_{\mathrm{dyn}} \propto \alpha_{\mathrm{vir}}^{-1/2}\,\mathrm{SFR}_{\mathrm{ff}}$. Elmegreen (2007) has criticized the evidence presented by Krumholz & Tan (2007), in support of his previous suggestion that the process of star formation lasts approximately 1–2 dynamical times on all scales (Elmegreen 2000). However, he defines the dynamical time as $1/(G\rho)^{1/2} = 0.54\tau_{\mathrm{ff,0}}$, assuming that the cloud internal velocity dispersion is of the order of the virial velocity, which implies $\mathrm{SFR}_{\mathrm{dyn}} = 0.54\,\mathrm{SFR}_{\mathrm{ff}}$.

In Krumholz & McKee (2005), the timescale for the collapse of the mass above the critical density is assumed to be proportional to $\tau_{\mathrm{ff,0}}$, with the constant of proportionality (ϕ_t in their Equation (19)) to be determined by comparison with numerical simulations. Our choice of a timescale equal to $\tau_{\mathrm{ff,cr}}$ is physically motivated, because structures of density equal to ρ_{cr} should collapse on that timescale. Because of our definite and physically motivated choice of the timescale, the prediction of our model with $\epsilon = 1$ should be interpreted as the maximum allowed SFR. The value of $\mathrm{SFR}_{\mathrm{ff}}$ in the simulations should never be larger than that. If it is smaller than the maximum rate predicted by the model, the reduction is absorbed by the efficiency factor ϵ, meaning that only a mass fraction ϵ of the gas with density above the critical one is found within gravitationally unstable regions.

In Section 7, we show that the SFR in our HD simulations achieves this predicted maximum value, for any value of α_{vir} we have tested ($\epsilon = 1$, independent of α_{vir}), while in the MHD simulations only approximately half of the magnetized gas above the critical density seems to be in collapsing regions ($\epsilon = 0.5$, independent of α_{vir}). Because the simulations are reproduced by the model with ϵ independent of α_{vir}, the timescale τ_{ff} in Krumholz & McKee (2005) is not a good choice, as it would require their coefficient ϕ_t to vary with α_{vir} (the relation $\tau_{\mathrm{ff,0}}/\tau_{\mathrm{ff,cr}} = x_{\mathrm{cr}}^{1/2} \sim \alpha_{\mathrm{vir}}^{1/2}$ shows that our model predicts a shallower dependence of $\mathrm{SFR}_{\mathrm{ff}}$ on α_{vir} than in Krumholz & McKee 2005).

Figure 3 shows the result of Equation (30) as a function of the virial parameter, for three values of the sonic Mach number, $\mathcal{M}_{S,0} = 4.5$, 9, and 18, in the MHD case, $\beta = 0.39$, and in the HD case ($\beta = \infty$). We have assumed a value of $\theta = 0.35$, as discussed in Section 2. In the HD case (dashed lines), we have assumed $\epsilon = 1$, while the curves for the MHD case (solid lines) are computed for $\epsilon = 0.5$. This choice of ϵ is motivated by the numerical results presented in Section 7.

Due to our timescale choice of $\tau_{\mathrm{ff,cr}}$ instead of $\tau_{\mathrm{ff,0}}$, the $\mathrm{SFR}_{\mathrm{ff}}$ is found to increase with increasing $\mathcal{M}_{S,0}$ (for constant virial parameter), while in Krumholz & McKee (2005) it decreases with increasing $\mathcal{M}_{S,0}$, as shown by their Figure 3 and by the power-law approximation, $\mathrm{SFR}_{\mathrm{ff}} \sim \mathcal{M}_{S,0}^{-0.32}$, in their Equation (30). We will show in Section 7 that the Mach number dependence of our model is confirmed by the star formation simulations.

---

[4] The integral in Equation (30) is solved assuming that the critical density is not strongly correlated with the local value of the density, or, equivalently, that the actual postshock thickness is not strongly correlated with the postshock density.

6
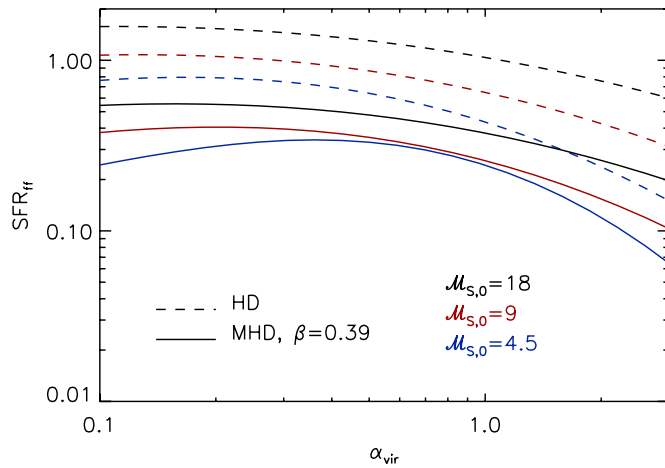
Figure 3. The star formation rate per free-fall time vs. the virial parameter according to Equation (30), for the HD case (dashed lines), and the MHD case with $\beta = 0.39$ (solid lines). In both cases, the three lines are for three different values of the sonic rms Mach number, $\mathcal{M}_{S,0} = 4.5$, 9, and 18, from bottom to top. In the MHD case, SFR_{ff} has been divided by a factor of two, in order to separate the MHD curves from the HD ones, and also because the star-formation simulations show that only half of the mass above the critical density can collapse in the MHD case, as shown in Section 7.

(A color version of this figure is available in the online journal.)

6. SFR IN SIMULATIONS OF DRIVEN MHD TURBULENCE

In order to test the SFR model, we have run a set of simulations of driven supersonic turbulence, on meshes with 500^3–1000^3 computational zones. Using the same methods and setup as in Padoan & Nordlund (2002, 2004), we adopt periodic boundary conditions, isothermal equation of state, and random forcing in Fourier space at wavenumbers $1 \leqslant k \leqslant 2$ ($k = 1$ corresponds to the computational box size). The simulations are all based on two initial snapshots of fully developed turbulence, one for HD and one for MHD. These snapshots are obtained by running the HD and the MHD simulations from initial states with uniform initial density and magnetic field, and random initial velocity field with power only at wavenumbers $1 \leqslant k \leqslant 2$, for approximately five dynamical times, on meshes with 1000^3 computational zones, with the driving force keeping the rms sonic Mach number at the approximate value of $\mathcal{M}_{S,0} = \sigma_{v,3D}/c_S \approx 9$. In the case of the HD run with $\mathcal{M}_{S,0} = 4.5$ (run HD10 in Table 1), the forcing was reduced prior to the inclusion of self-gravity until the targeted Mach number was reached.

In the MHD simulation, the initial magnetic field is such that the initial value of the ratio of gas to magnetic pressure is $\beta_0 = 22.2$. At the time when the gravitational force is included, the magnetic field has been amplified by the turbulence, and the value of β is $\beta = 2c_S^2/\langle B^2/4\pi\rho \rangle = 0.33$, consistent with Equation (20) with $b = 0.63$, using the mean-squared v_A averaged in regions with density larger than twice the mean, and $\beta = 0.11$, consistent with Equation (20) with $b = 0.22$, using the mean-squared v_A averaged over the whole domain.

The star formation simulations start when the gravitational force is included. The computational mesh is downsized from 1000^3 to 500^3 zones for the 500^3 runs or kept the same for the 1000^3 runs. The driving force is still active during the star formation phase of the simulations, in order to achieve a stationary value of α_{vir} to correlate with the SFR.

An example of a projected density field from a star formation simulation is shown in Figure 4. Table 1 gives the values of the sonic rms Mach number, $\mathcal{M}_{S,0}$, the initial pressure ratio, β_0, the Jeans length in units of the box size, $L_J/L_0 \approx 1.94\, \alpha_{vir}^{1/2} \mathcal{M}_{S,0}^{-1}$, the virial parameter, α_{vir}, and the SFR per free-fall time, SFR_{ff}, for all the 19 simulations used to test the theoretical model.

Our simulations represent an intermediate range of scales. The forcing represents the inertial forcing from scales larger than the box size. These larger scale motions have longer turnover times—and hence longer lifetimes—than the turnover times of the scales covered by the simulations. They act to maintain the kinetic energy on smaller scales. Without the corresponding driving, the motions on the scales covered by the simulations would decay, which would lead to a lowering of the virial parameter and a corresponding secular increase in the SFR. By maintaining the driving we avoid the secular evolution and obtain a consistent and nearly constant SFR.

The virial parameter defined in Equation (1) is for a sphere of uniform density. The simulations are carried out in a cubic domain and generate a highly nonlinear density field; real star-forming regions have irregular shapes and are highly fragmented. The virial parameter of the simulations, as well as that of real molecular clouds, is therefore only an approximation of the energy ratio. To define the virial parameter of the simulations, we have chosen to use Equation (1), with $R = L_0/2$, where L_0 is the box size, and M is equal to the total mass in the box, M_0. The virial parameter is then $\alpha_{vir} = 5\, v_0^2\, L_0/(6\, G M_0)$, where v_0 is the three-dimensional rms velocity in the box.

A collapsing region is captured by the creation of an accreting sink particle if the density exceeds a certain density threshold (8000 times the mean density in both 500^3 and 1000^3 runs). We have verified that the largest density reached by non-collapsing regions is always much smaller than that value, so only a collapsing region can create a sink particle. No other conditions need to be satisfied to identify genuine collapsing regions. Once a particle is created its subsequent motion is followed, allowing for influences from the gravitational potential and from accretion. When calculating the gravitational potential, the masses of the stars are added back into a fiducial density field, using narrow Gaussian profiles ($1/e$ radius 1.15 grid zones) to represent the sink particles. The Poisson equation for the gravitational potential is solved using parallelized fast Fourier transforms with Gaussian softening ($1/e$ radius $2\sqrt{2}$ grid zones).

Further accretion (defined as density exceeding the density threshold) is collected onto the nearest sink particle if the distance is less than four grid zones. Sink particles are not merged, and thus maintain their identity even if they become trapped in the same potential well (the softening of the gravitational potential ensures that no singularity occurs).

In Figures 5 and 6, we show the SFE versus time in the HD and MHD simulations, respectively. The SFE is defined as the mass in sink particles divided by the total initial mass. The time is given in units of the free-fall time of each simulation, so the slope of the plots corresponds to the SFR_{ff}. The plots only show the SFE from the time when the first sink particle is created, which is some time after the gravity is turned on. The time to the formation of the first sink particles is longer for simulations with larger α_{vir}, which cannot be appreciated in Figures 5 and 6.

Even after the first sink particle is created, there is still an initial transient phase with increasing SFR. This transient phase usually lasts until SFE ≈ 0.03. The SFR_{ff} is therefore estimated as the slope of a least-square fit to the SFE in the interval
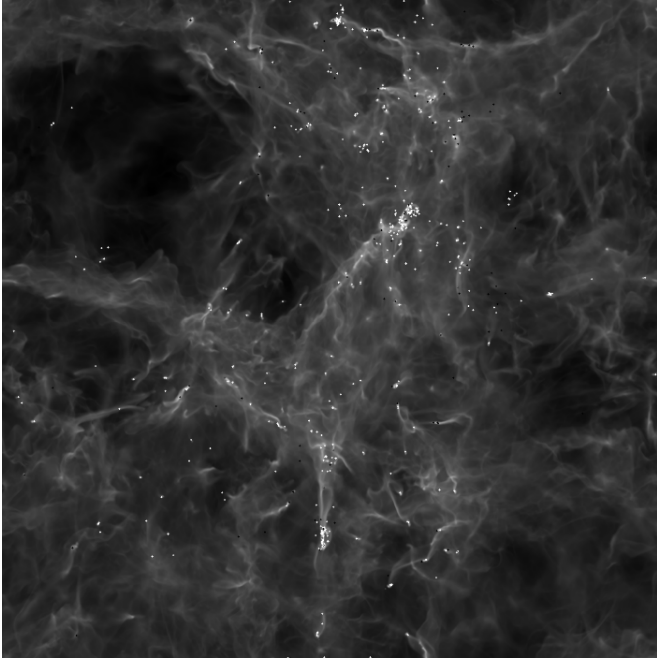
Figure 4. Logarithm of projected density from a snapshot of an exploratory 1000^3 run with $\beta_0 = 22.2$, $\mathcal{M}_{S,0} = 18$, and $\alpha_{vir} = 0.9$, at a time when approximately 10% of the mass has been converted into stars. Bright dots show the positions of the stars (sink particles), while black dots are for brown dwarfs (some of which are still accreting and may later grow to stellar masses).

Table 1
Non-dimensional Parameters of the Simulations Used to Measure the Star Formation Rate

Run	N	$\mathcal{M}_{S,0}$	β_0	L_J/L_0	α_{vir}	SFR$_{ff}$
HD1	500^3	9.0	∞	0.10	0.22	1.01
HD2	500^3	9.0	∞	0.12	0.34	0.86
HD3	500^3	9.0	∞	0.15	0.48	0.86
HD4	500^3	9.0	∞	0.18	0.67	0.75
HD5	500^3	9.0	∞	0.21	0.95	0.68
HD6	500^3	9.0	∞	0.25	1.33	0.51
HD7	500^3	9.0	∞	0.31	2.04	0.29
HD8	1000^3	9.0	∞	0.21	0.95	0.71
HD9	1000^3	9.0	∞	0.31	2.04	0.41
HD10	500^3	4.5	∞	0.18	0.67	0.54
MHD1	500^3	9.0	22.2	0.10	0.22	0.43
MHD2	500^3	9.0	22.2	0.12	0.34	0.42
MHD3	500^3	9.0	22.2	0.15	0.48	0.39
MHD4	500^3	9.0	22.2	0.18	0.67	0.31
MHD5	500^3	9.0	22.2	0.21	0.95	0.19
MHD6	500^3	9.0	22.2	0.25	1.33	0.15
MHD7	500^3	9.0	22.2	0.31	2.04	0.05
MHD8	1000^3	9.0	22.2	0.21	0.95	0.20
MHD9	1000^3	9.0	22.2	0.31	2.04	0.15

$0.03 \leqslant$ SFE $\leqslant 0.2$. The SFR based on this interval of the SFE is quite robust with respect to changes in the treatment of sink particles (threshold density, accretion radius, gravitational softening, etc.); even changes that affect the number of sink particles significantly do not change the measured SFR much.

All runs were continued until SFE $\geqslant 0.4$, and some until SFE ≈ 0.8. However, we prefer to fit the SFR only up to SFE $= 0.2$, because larger values are rarely found in star-forming regions, and because the simulations should not be trusted past that point (the stellar content may start to affect the gas motion, and the gravitational interactions in close encounters between sink particles are not accurately computed with an N-body code).

Figures 5 and 6 show that SFR$_{ff}$ decreases monotonically with increasing α_{vir} ($\alpha_{vir} = 0.22$–2.04 for the plots from top to bottom). It is well defined because the SFE plots are almost straight lines (constant instantaneous SFR) for almost all the simulations, except for a tendency of some of the MHD runs to slightly increase their SFR also at relatively high values of SFE. The MHD run with the highest virial parameter, $\alpha_{vir} = 2.04$ (MHD7 in Table 1), has the lowest SFR and shows a rather episodic SFE evolution. However, its mean SFR$_{ff}$ in the range $0.03 \leqslant$ SFE $\leqslant 0.2$ is well defined.

7. MODELS VERSUS NUMERICAL RESULTS

Figure 7 compares the SFR model with the numerical results. It shows SFR$_{ff}$ versus α_{vir} for all the simulations listed in Table 1, and for the HD (dashed and dotted lines) and MHD (solid line) models. The model prediction corresponds to Equation (30), with $\epsilon = 1.0$ in the HD case, and $\epsilon = 0.5$, in the MHD case.

The HD simulations follow almost exactly the theoretical prediction with $\epsilon = 1$, suggesting that all the gas with density above the critical value collapses in a timescale of order $\tau_{ff,cr}$, as assumed in the model. The dependence of SFR$_{ff}$ on α_{vir} is too shallow to be consistent with the parameterization in Krumholz

& McKee (2005), where the timescale is $\phi_t \tau_{ff,0}$, unless ϕ_t is allowed to change with the virial parameter, $\phi_t \propto \alpha_{vir}^{1/2}$.

Of the 500^3 HD runs, only the one with the highest α_{vir} (HD7) deviates significantly ($\approx 50\%$) from the theoretical prediction. However, the corresponding higher resolution run yields a higher value of SFR$_{ff}$, nearly identical to the theoretical prediction. At $\alpha_{vir} = 0.95$, instead, the 500^3 run is already converged to the SFR of the corresponding 1000^3 run (HD5 and HD8, respectively). The run with the highest value of α_{vir} is expected to be the one requiring the largest numerical resolution, because $\rho_{cr,HD}/\rho_0 \propto \alpha_{vir}$, according to Equation (8). In other words, higher α_{vir} can be interpreted as lower mean density (everything else remaining unchanged), making it harder to reach the critical density for collapse in the simulation.

The HD runs also confirm the theoretical prediction that SFR$_{ff}$ should increase with increasing $\mathcal{M}_{S,0}$ (the opposite of the prediction in Krumholz & McKee 2005), as shown by the comparison of runs HD4 and HD10, with $\mathcal{M}_{S,0} = 4.5$ and 9, respectively. The lower Mach number run fits the theoretical prediction very well, confirming our choice of $\tau_{ff,cr}$ for the timescale of star formation.

Similar considerations apply to the MHD runs. There is good agreement between the simulations and the theoretical model with $\epsilon = 0.5$, although the model predicts a significantly higher SFR than the 500^3 simulation with the largest value of α_{vir}. This discrepancy may be entirely due to the insufficient numerical resolution of the simulation, because the 1000^3 run with the same virial parameter, $\alpha_{vir} = 2.04$, yields a value of SFR$_{ff}$ almost identical to the theoretical prediction. As in the HD simulations, the case with $\alpha_{vir} = 0.95$ seems to be already converged at a resolution of 500^3 computational zones, as its SFR$_{ff}$ is nearly identical to that of the corresponding 1000^3 run (and only approximately 20% below the predicted value).

The value of $\epsilon = 0.5$ derived from the comparison of the model with the MHD simulations can be understood with the following argument. In the MHD case, the critical mass for collapse depends on both the local density and the local magnetic field strength, B, while in HD it depends only on the local density (assuming constant temperature). In HD, regions with
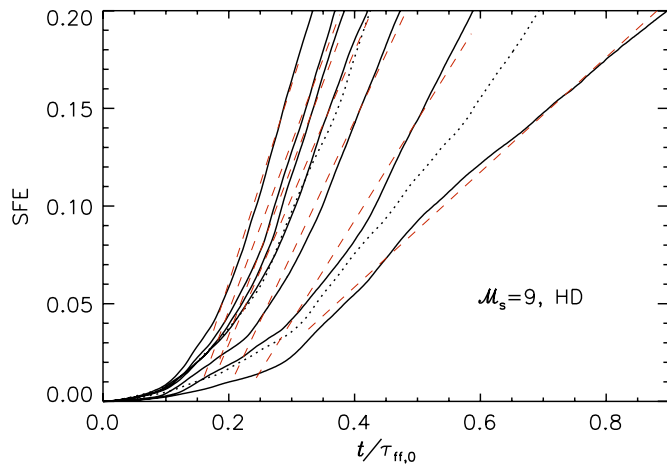
Figure 5. Star formation efficiency vs. time for all the HD runs with $\mathcal{M}_{S,0} = 9$ listed in Table 1. The star formation efficiency is defined as the mass in stars (sink particles) divided by the total mass, and the time is in units of the free-fall time of the mean density of each simulation, $\tau_{\rm ff,0}$. The dashed lines show the least-squares fit to each curve between SFE = 0.03 and SFE = 0.2. The slope of those linear fits defines the SFR$_{\rm ff}$ plotted in Figure 7. The two dotted curves are from the 1000^3 runs (HD8 and HD9). The value of $\alpha_{\rm vir}$ for each curve varies from 0.22 to 2.04 (see Table 1) from top to bottom.

(A color version of this figure is available in the online journal.)

density larger than the critical value must collapse, because of the lack of gas pressure support. In the MHD case, instead, at any density value there is a large scatter in B. Even if the local density is above the critical value, the pressure support is dominated by magnetic pressure, and, due to the large scatter in B (and even larger in B^2), a region with B larger than the mean value at that density may be prevented from collapsing. The value $\epsilon = 0.5$ is reasonable, because the critical density is derived with characteristic postshock values, and it is possible that in half of the cases the magnetic field deviates enough from its characteristic postshock value to prevent the gravitational collapse.

8. DISCUSSION

8.1. The Timescale of Star Formation

We have modeled the SFR assuming that a mass fraction ϵ of all regions with density larger than the critical one is converted into stars in a time $\tau_{\rm ff,cr}$. To maintain this SFR over a time longer than $\tau_{\rm ff,cr}$, the turbulent flow must continuously "regenerate" the high-density tail of the gas density pdf, on a timescale shorter than or equal to $\tau_{\rm ff,cr}$. This may seem unlikely, because in super-Alfvénic turbulence the global dynamical time is always longer than the collapse time of the unstable regions, $\tau_{\rm dyn} > \tau_{\rm ff,cr}$. For example, $\tau_{\rm ff,cr}/\tau_{\rm dyn} = 4.6\,\theta\,\mathcal{M}_{S,0}^{-1}(1+\beta^{-1})/(1+0.925\beta^{-3/2})^{1/3} = 0.34$ and 0.16, for $\beta = 0.39$ and $\beta \to \infty$, respectively, assuming $\mathcal{M}_{S,0} = 10$. However, the turbulence can "regenerate" the high-density tail of the pdf sufficiently rapidly, because the collapsing dense regions account for only a very small fraction of the total mass. The turbulent flow "processes" a gas mass of the order of the total mass in one dynamical time (think of the trivial example of a single shock crossing the whole volume in one dynamical time), hence, a mass fraction of order $\tau_{\rm ff,cr}/\tau_{\rm dyn}$ in a time equals to $\tau_{\rm ff,cr}$. At a characteristic Mach number value of $\mathcal{M}_{S,0} = 10$, this mass fraction is always larger than 0.16 (the value found above for the extreme limit of $\beta \to \infty$). The mass fraction above the critical density is typically much smaller than that of order a few per cent. If the
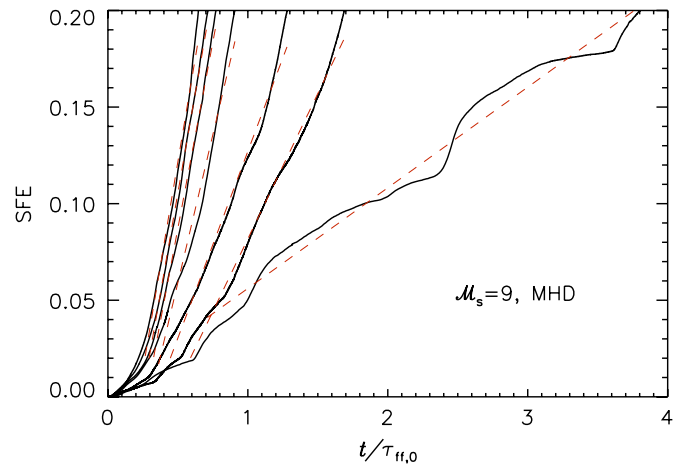
**Figure 6.** Same as Figure 5, but for the MHD simulations.

(A color version of this figure is available in the online journal.)

critical density is increased, the mass fraction processed by the turbulence in a time $\tau_{\rm ff,cr}$ decreases as $\rho_{\rm cr}^{-1/2}$, while the mass fraction above the critical density drops more rapidly, due to the lognormal nature of the pdf. Therefore, the collapse of regions with density above the critical value can be continuously "fed" by the turbulence, and our choice of $\tau_{\rm ff,cr}$ as the star formation timescale is justified.

The above argument also means that the collapse of unstable regions of densities $\rho > \rho_{\rm cr}$ is not expected to strongly affect the density pdf at densities $\rho \lesssim \rho_{\rm cr}$. We have verified that, once star formation is initiated by the inclusion of self-gravity, the density pdf in our simulations develops a power-law tail $\propto \rho^{-3/2}$ at densities $\rho \gtrsim \rho_{\rm cr}$, a signature of free fall, while it maintains the lognormal shape for $\rho < \rho_{\rm cr}$. The rapid mass processing by the turbulence that allows the preservation of the lognormal pdf despite the effect of self-gravity explains why it is possible to predict the SFR based on the statistics of turbulence alone, with no modification due to self-gravity. One can model the process of star formation with two distinct phases: the formation of dense regions by turbulent compressions and the gravitational collapse of the densest of those regions. Locally, this is roughly what happens, while globally, the turbulence and the gravity are always operating at the same time.

8.2. SFR in Molecular Clouds

Krumholz & Tan (2007) argue that SFR$_{\rm ff} \sim 0.02$ in a variety of star-forming environments, spanning approximately four orders of magnitude in gas density. The estimated values of SFR have large error bars, but the lack of a strong density dependence would suggest that most star-forming regions have a comparable value of $\alpha_{\rm vir}$. More recently, Evans et al. (2009) have estimated values of SFR$_{\rm ff}$ in giant molecular clouds (GMCs) and within some of the dense cloud cores. They find values significantly larger than the characteristic one in Krumholz & Tan (2007). They obtain SFR$_{\rm ff} = 0.03$–0.06 for GMCs with mean densities distributed around a mean value of $\langle n \rangle = 390\,{\rm cm}^{-3}$ (and SFE in the range 0.03–0.06 as well), and SFR$_{\rm ff} = 0.05$–0.25 for dense cores with mean densities 50–200 times those of the GMCs (and SFE of approximately 0.5). These values are computed by assuming that all the stars detected (by their infrared excess) have been formed in the last 2 Myr. The authors report a best estimate of 2 ± 1 Myr for the lifetime of the Class II phase, meaning that the SFR$_{\rm ff}$ could be 50% lower, or 100% higher
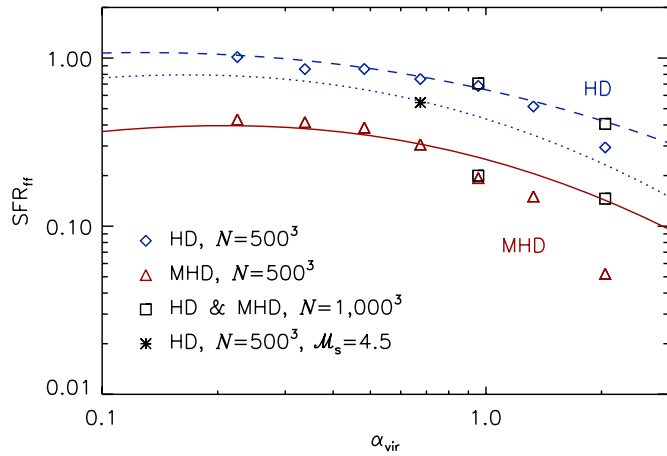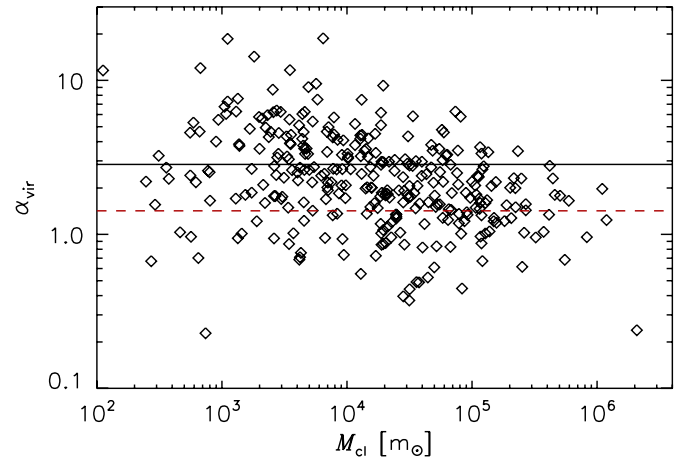
Figure 7. Star formation rate per free-fall time vs. virial parameter for the 500^3 MHD simulations (triangles) and for the 500^3 HD simulations (diamonds) with $\mathcal{M}_{S,0} = 9$. The squares are for the 1000^3 runs, and the asterisk for the 500^3 HD run with $\mathcal{M}_{S,0} = 4.5$. The MHD model with $\mathcal{M}_{S,0} = 9$ and $\beta = 0.39$ is shown by the solid line. The HD model ($\beta_0 = \infty$) is shown by the dashed line for $\mathcal{M}_{S,0} = 9$ and by the dotted line for $\mathcal{M}_{S,0} = 4.5$. The values of SFR_{ff} from the simulations are the slopes of the linear fits to the SFE vs. time between SFE $= 0.03$ and SFE $= 0.2$ (see Figures 5 and 6). The values of SFR_{ff} of the models are from Equation (30), with $\epsilon = 1.0$ in the HD case, and $\epsilon = 0.5$ for the MHD model.

(A color version of this figure is available in the online journal.)

Figure 8. Virial parameter vs. cloud mass from Heyer et al. (2009). All 316 objects from their Table 1 are shown, including those selected within the smaller maps of area A_2. The horizontal solid line marks the mean value of $\alpha_{vir} = 2.8$, and the dashed line half that value, $\alpha_{vir} = 1.4$, assuming that the LTE-derived mass underestimates the true mass by a factor of two, causing an overestimate of the virial parameter by the same factor.

(A color version of this figure is available in the online journal.)

than the values given above. Accounting for this uncertainty, one gets $SFR_{ff} = 0.02$–0.12 for GMCs, and $SFR_{ff} = 0.03$–0.5 for dense cores, suggesting a characteristic value of order 0.1, rather than 0.01. Evans et al. (2009) suggest that the SFR in dense cores would be lower, if one assumed that the total mass in the cores was larger when the star formation process started than at present. However, it is also possible that star formation was already occurring while the cores were still being assembled by flows accreting from the larger scale. In this case, the initial core mass may have been smaller than the current one, resulting in an SFR larger than estimated.

Figure 3 shows that for a range of values of $\mathcal{M}_{S,0}$ characteristic of MCs, we predict $SFR_{ff} \approx 0.12$–0.28 at $\alpha_{vir} = 2$. These values should be reduced by a factor of two or three (Matzner & McKee 2000; André et al. 2010), to account for mass loss from stellar outflows and jets, not included in the model and in the simulations. With this reduction, our results are consistent with the relatively high values of SFR_{ff} found by Evans et al. (2009). Another source of uncertainty lies in the mapping of our definition of the virial ratio for a periodic box (Equation (1)) to the virial ratios used to characterize observed star-forming regions. One example is the estimate of the characteristic α_{vir} of GMCs. Heyer et al. (2009) have recently studied again a large subset of the GMCs sample of Solomon et al. (1987). For each cloud, they compute LTE masses based on the $J = 1$–0 emission lines of ^{13}CO and ^{12}CO. They find masses smaller by a factor of 2–5 than the virial masses derived by Solomon et al. (1987). Their revised velocity dispersion is also somewhat smaller than in Solomon et al. (1987), but their resulting virial parameters are still a factor of approximately 2–3 larger.

Figure 8 shows α_{vir} versus the cloud mass, M_{cl}, for all their 316 maps (including the smaller ones of area A_2). The mean value of the virial parameter is $\alpha_{vir} = 2.8 \pm 2.4$. If the LTE-derived mass underestimates the real mass by a factor up to two, as argued by the authors, then the values of α_{vir} should be reduced by a factor of two. The mean value is therefore

likely to lie in the range $\alpha_{vir} = 1.4$–2.8, but with a very large scatter. As commented above, if GMCs have a characteristic value of $\alpha_{vir} \approx 2$, as suggested by this observational sample, the SFR predicted by our model for a reasonable range of values of $\mathcal{M}_{S,0}$, and accounting for a factor of two or three reduction due to mass-loss in outflows and jets, may be consistent with the recent observational estimates by Evans et al. (2009).

9. SUMMARY AND CONCLUDING REMARKS

This work presents a new physical model of the SFR that could be implemented in galaxy formation simulations. The model depends on the relative importance of gravitational, turbulent, magnetic, and thermal energies, expressed through the virial parameter, α_{vir}, the rms sonic Mach number, $\mathcal{M}_{S,0}$, and the ratio of the mean gas pressure to mean magnetic pressure, β_0. The value of SFR_{ff} is predicted to decrease with increasing α_{vir}, and to increase with increasing $\mathcal{M}_{S,0}$, for values typical of star-forming regions ($\mathcal{M}_{S,0} \approx 4$–$20$). In the complete absence of a magnetic field, SFR_{ff} increases typically by a factor of three, proving the importance of magnetic fields in star formation, even when they are relatively weak (super-Alfvénic turbulence).

In the non-magnetized limit, our definition of the critical density for star formation has the same dependence on α_{vir} and $\mathcal{M}_{S,0}$ as in the model of Krumholz & McKee (2005), but our physical derivation does not rely on the concepts of local turbulent pressure and sonic scale. Due to our different choice of star formation timescale (see Section 8.1), our model predicts a different dependence of the SFR on α_{vir} and $\mathcal{M}_{S,0}$ from the model of Krumholz & McKee (2005). The model predictions have been tested with an unprecedented set of large numerical simulations of supersonic MHD turbulence, including the effect of self-gravity, and capturing collapsing cores as accreting sink particles. The SFR in the simulations follows closely the theoretical predictions.

Although based on reasonable physical assumptions, this phenomenological model of the SFR bypasses the great complexity of the nonlinear dynamics of supersonic, self-gravitating, mag-

netized turbulence, by taking advantage of the gas density pdf of fully developed turbulence. Because it provides a prediction of the SFR based solely on turbulence statistics, with no correction for the effect of self-gravity, the model shows that the process of star formation may be envisioned as the effect of two almost independent steps: (1) turbulent fragmentation, with little influence from self-gravity, and (2) the local collapse of the densest regions, with little influence from turbulence. This approximation is a basic assumption in the stellar IMF model of Padoan & Nordlund (2002) as well. It is also fundamentally different from the assumptions of star formation models relying on the concept of local turbulent pressure support, where the local competition between turbulence and self-gravity is always important on all scales.

This work illustrates how the turbulence controls the SFR. It does not address how the turbulence is driven to a specific value of $\alpha_{\rm vir}$. Because much of the turbulence driving is likely due to SN explosions, the turbulent kinetic energy and the value of $\alpha_{\rm vir}$ are coupled to the SFR in a feedback loop. The feedback determines the equilibrium level of the SFR (and hence also the equilibrium level of $\alpha_{\rm vir}$) at large scales. If $\alpha_{\rm vir}$ were to decrease (increase) relative to the equilibrium, the SFR would increase (decrease), according to the results of this work, resulting in an increased (decreased) energy injection rate by SN explosions, thus restoring a higher (lower) value of $\alpha_{\rm vir}$. The dependence of the SFR on $\alpha_{\rm vir}$ found in this work suggests that this self-regulation may work quite effectively.

Cosmological simulations of galaxy formation provide the rate of gas cooling and infall, which sets the gas reservoir for the star formation process and thus ultimately controls the SFR. They also include prescriptions for the star formation feedback, known to be essential to recover observed properties of galaxies (Gnedin et al. 2009; Gnedin & Kravtsov 2010). Future galaxy formation simulations should adopt a physical SFR law with an explicit dependence on $\alpha_{\rm vir}$, $\mathcal{M}_{\rm S,0}$, and β as derived in this work, in order to correctly reflect specific conditions of protogalaxies at different redshifts. This requires a treatment of the star formation feedback capable of providing an estimate of $\alpha_{\rm vir}$ on scales of order 10–100 pc, not far from the spatial resolution currently achieved by the largest cosmological simulations of galaxy formation.

REFERENCES

André, P., et al. 2010, A&A, 518, L102
Beetz, C., Schwarz, C., Dreher, J., & Grauer, R. 2008, Phys. Lett. A, 372, 3037
Bertoldi, F., & McKee, C. F. 1992, ApJ, 395, 140
Bonazzola, S., Falgarone, E., Heyvaerts, J., Perault, M., & Puget, J. L. 1987, A&A, 172, 293
Bonazzola, S., Perault, M., Puget, J. L., Heyvaerts, J., Falgarone, E., & Panis, J. F. 1992, J. Fluid Mech., 245, 1
Bonnor, W. B. 1956, MNRAS, 116, 351
Brunt, C. M., Federrath, C., & Price, D. J. 2010, MNRAS, 403, 1507
Chandrasekhar, S. 1951, Proc. R. Soc. A, 210, 26
Crutcher, R. M. 1999, ApJ, 520, 706
de Avillez, M. A., & Breitschwerdt, D. 2005, A&A, 436, 585
Ebert, R. 1957, Z. Astrophys., 42, 263
Elmegreen, B. G. 2000, ApJ, 530, 277
Elmegreen, B. G. 2007, ApJ, 668, 1064
Evans, N. J., et al. 2009, ApJS, 181, 321
Falgarone, E., Troland, T. H., Crutcher, R. M., & Paubert, G. 2008, A&A, 487, 247
Federrath, C., Klessen, R. S., & Schmidt, W. 2008, ApJ, 688, L79
Gnedin, N. Y., & Kravtsov, A. V. 2010, ApJ, 714, 287
Gnedin, N. Y., Tassis, K., & Kravtsov, A. V. 2009, ApJ, 697, 55
Hennebelle, P., & Chabrier, G. 2008, ApJ, 684, 395
Heyer, M. H., & Brunt, C. M. 2004, ApJ, 615, L45
Heyer, M. H., Krawczyk, C., Duval, J., & Jackson, J. M. 2009, ApJ, 699, 1092
Joung, M. K. R., & Mac Low, M.-M. 2006, ApJ, 653, 1266
Kim, J., Balsara, D., & Mac Low, M.-M. 2001, J. Korean Astron. Soc., 34, 333
Korpi, M. J., Brandenburg, A., Shukurov, A., Tuominen, I., & Nordlund, Å. 1999, ApJ, 514, L99
Kritsuk, A. G., Norman, M. L., Padoan, P., & Wagner, R. 2007, ApJ, 665, 416
Kritsuk, A. G., Ustyugov, S. D., Norman, M. L., & Padoan, P. 2009a, J. Phys. Conf. Ser., 180, 012020
Kritsuk, A. G., Ustyugov, S. D., Norman, M. L., & Padoan, P. 2009b, in ASP Conf. Ser. 406, Numerical Modeling of Space Plasma Flows, ed. N. V. Pogorelov et al. (San Francisco, CA: ASP), 15
Krumholz, M. R., & McKee, C. F. 2005, ApJ, 630, 250
Krumholz, M. R., & Tan, J. C. 2007, ApJ, 654, 304
Larson, R. B. 1981, MNRAS, 194, 809
Lemaster, M. N., & Stone, J. M. 2008, ApJ, 682, L97
Li, P. S., Norman, M. L., Mac Low, M.-M., & Heitsch, F. 2004, ApJ, 605, 800
Lunttila, T., Padoan, P., Juvela, M., & Nordlund, Å. 2008, ApJ, 686, L91
Lunttila, T., Padoan, P., Juvela, M., & Nordlund, Å. 2009, ApJ, 702, L37
Matzner, C. D., & McKee, C. F. 2000, ApJ, 545, 364
McKee, C. F. 1989, ApJ, 345, 782
McKee, C. F., & Ostriker, E. C. 2007, ARA&A, 45, 565
Nakano, T., & Nakamura, T. 1978, PASJ, 30, 671
Nordlund, Å., & Padoan, P. 1999, in Interstellar Turbulence, ed. J. Franco & A. Carramiñana (Cambridge: Cambridge Univ. Press), 218
Ostriker, E. C., Stone, J. M., & Gammie, C. F. 2001, ApJ, 546, 980
Padoan, P. 1995, MNRAS, 277, 377
Padoan, P., Juvela, M., Goodman, A. A., & Nordlund, Å. 2001, ApJ, 553, 227
Padoan, P., & Nordlund, Å. 1999, ApJ, 526, 279
Padoan, P., & Nordlund, Å. 2002, ApJ, 576, 870
Padoan, P., & Nordlund, Å. 2004, ApJ, 617, 559
Padoan, P., Nordlund, Å., & Jones, B. 1997, MNRAS, 288, 145
Solomon, P. M., Rivolo, A. R., Barrett, J., & Yahil, A. 1987, ApJ, 319, 730
Tamburro, D., Rix, H.-W., Leroy, A. K., Low, M.-M. M., Walter, F., Kennicutt, R. C., Brinks, E., & de Blok, W. J. G. 2009, AJ, 137, 4424
Tomisaka, K., Ikeuchi, S., & Nakamura, T. 1988, ApJ, 335, 239
Troland, T. H., & Crutcher, R. M. 2008, ApJ, 680, 457
Vazquez-Semadeni, E. 1994, ApJ, 423, 681
Vázquez-Semadeni, E., Ballesteros-Paredes, J., & Klessen, R. S. 2003, ApJ, 585, L131
Vázquez-Semadeni, E., Kim, J., & Ballesteros-Paredes, J. 2005, ApJ, 630, L49
Wang, H., & George, W. K. 2002, J. Fluid Mech., 459, 429
Williams, J. P., & McKee, C. F. 1997, ApJ, 476, 166
Zuckerman, B., & Palmer, P. 1974, ARA&A, 12, 279